REFERENCES

1. C. M. Maritan, L. P. Berndt, N. G. Tarr, M. J. Bullerwell, and J. M. Jenkins, *This Journal*, **135**, 1793 (1988).
2. L. H. Hall and M. Koliwad, *ibid.*, **120**, 1438 (1973).
3. C. A. Chang, *ibid.*, **123**, 1245 (1976).
4. F. C. Everstein and B. H. Put, *ibid.*, **120**, 106 (1973).
5. D. Bielle-Daspet, F. Mansour-Bahloul, A. Martinez, B. Pieraggi, B. de Mauduit, A. Oustry, R. Carles, G. Landa, F. Ajustron, A. Mazel, and P. Riboulet, *Thin Solid Films*, **150**, 69 (1987).
6. D. Bielle-Daspet, E. Scheid, C. Azzaro, B. de Mauduit, and B. Pieraggi, *ibid.*, **204**, 33 (1991).
7. C. Azzaro, E. Scheid, D. Bielle-Daspet, P. Duverneuil, and P. Boudre, in *Proceedings of the 8th Conference on CVD, J. Chim. Phys. II*, **1**, p. C2 (1991).
8. J. H. Purnell and W. Walsh, *Proc. R. Soc. London Series A*, **293**, 543 (1966).
9. P. John and J. H. Purnell, *J. Chem. Soc., Faraday Trans.*, **169**, 1455 (1973).
10. M. E. Coltrin, R. J. Kee, and J. A. Miller, *This Journal*, **131**, 425 (1984).
11. C. Azzaro, Ph.D. Thesis, INPT Toulouse, France (1991).
12. K. F. Jensen and D. B. Graves, *This Journal*, **139**, 1951 (1983).
13. K. F. Roenigk and K. F. Jensen, *ibid.*, **132**, 448 (1985).
14. T. E. Wilke, K. Turner, and C. J. Takousis, *Chem. Eng. Sci.*, **41**, 643 (1986).
15. M. E. Collingham and R. L. Zollars, *This Journal*, **136**, 787 (1989).
16. M. G. Joshi, *ibid.*, **134**, 3118 (1987).
17. S. Middleman and A. Yeckel, *ibid.*, **133**, 1951 (1986).
18. C. Azzaro, P. Duverneuil, and J. P. Couderc, *Chem. Eng. Sci.*, **47**, 3827 (1992).
19. G. Fresquet, CNAM Thesis, France (1991).
20. H. H. Lee, *J. Cryst. Growth*, **69**, 82 (1984).
21. W. A. P. Claassen and J. Bloem, *This Journal*, **128**, 1353 (1981).
22. C. Jacquemin, *Technical Report, Motorola*, Toulouse, France (1986).
23. M. Luthard, E. Than, and G. Marx, *Z. Chem.*, **22**, 231 (1982).
24. C. Azzaro, G. Fresquet, and J. P. Couderc, in *Proceedings of the 4th Congrès de Génie des Procédés, Récents progrès en génie des procédés*, Tech. Doc. Lavoisier, Editor, p. 127, Paris (1993).

On the Anisotropically Etched Bonding Interface of Directly Bonded (100) Silicon Wafer Pairs

B. K. Ju, Y. H. Lee, K. H. Tchah,[a] and M. H. Oh

Division of Electronics and Information Technology, Korea Institute of Science and Technology, 39-1 Haweolgog-dong, Seongbuk-gu, Seoul 136-791, Korea

[a]Department of Electronic Engineering, Korea University, Anam-dong, Seongbuk-gu, Seoul 136-701, Korea

ABSTRACT

We discovered that the shapes of the (111) facet structures were closely related to the disintegration, the spheroidization, and the stabilization of the native interfacial oxide layer in directly bonded Si wafer pairs. These (111) facet structures are generated from the anisotropic etching of (110) cross section of bonded (100) Si wafer pairs. After etching, the facet structures at the bonding interface look like a broken line as the interfacial oxide layers are disintegrated and spheroidized. When a uniform interfacial oxide layer is inserted between two silicon wafers, the oxide layer acts as an etch mask during anisotropic etching. Therefore, the (111) facet structure becomes wider and more pronounced. Also, we confirmed that most of the interfacial oxide existing at the bonding interface of well-aligned wafer pairs were disintegrated and spheroidized through a high temperature annealing process >900°C. Finally, we inferred from our measurements, the bonding strength (surface energy) increased as the interfacial oxide is stabilized, disintegrated, and spheroidized.

Introduction

In the silicon direct bonding process, it is essential to investigate voids (bubbles or noncontacted area)[1-3] and bonding strength of bonded silicon wafers,[1,3] and the condition of the interfacial oxide layer[4-11] for the application to silicon-on-insulator, silicon sensors, and power devices. Historically, researchers have employed various techniques for the investigation. Thermal (infrared) imaging technique, ultrasound microscopy, x-ray topography, magic mirror method, wafer gradual thinning method, and KOH etch-based method have been developed to observe macro- and microvoids.[1-3,12,13] To measure the bonding strength, the hydrostatic oil pressure method, the crack propagation method, and the tensile strength meter were employed.[14-16]

However, for studying the conditions of the interfacial oxide layer, the previously employed techniques are not satisfactory. That is, many researchers have used high resolution transmission electron microscopy (HRTEM) as a tool to observe very thin oxide layers.[4-11] Consequently, they cannot present a comprehensive picture since their results are limited to a very small area. Moreover, the preparation of samples is somewhat tedious, and so the number of samples for TEM observation is limited. These difficulties in TEM experiments can be illustrated by the fact that different researchers have reported contradicting results regarding the condition of the interfacial oxide.

To investigate the condition of interfacial oxide layer, we employed the KOH etch-based technique which is useful in observing voids as reported by Mitani *et al.*[3] They anisotropically etched the bonding interface using KOH-H_2O solution and discovered (111) facets on a (110) cross section for well-bonded (100) wafer pairs. They hypothesized that the oxide layer at the interface plays the role of etch mask which leaves (111) facet structures after etching. They also claimed that, when the native oxide was removed by dipping the wafers into an HF solution before bonding, no (111) facets were found at the bonded (110) cross section after KOH etching.

However, contrary to their claim, we found that the (111) facets exist at the (110) cross section of the bonded (100) wafer pairs even after HF dipping, and the presence of a native oxide layer cannot explain the generation mechanism of the facets completely. Based on scanning electron microscopy (SEM) and HRTEM observations, we discovered that a close relationship exists between the shape of (111) facets and the interfacial oxide conditions. Further, our improved KOH etching technique using both SEM and TEM can offer a more reliable and comprehensible picture of the condition of the interfacial oxide. Finally, we discuss the influence of the interfacial oxide condition on the bonding strength.

Downloaded on 2014-03-19 to IP 163.152.61.222 address. Redistribution subject to ECS terms of use (see ecsdl.org/site/terms_use) unless CC License in place (see abstract).

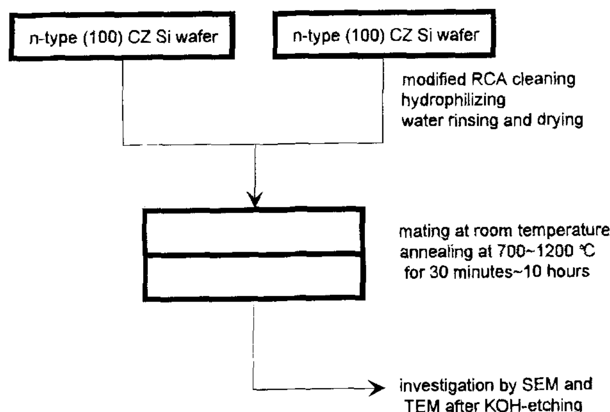

Fig. 1. Schematic diagram of Si wafer bonding procedure.

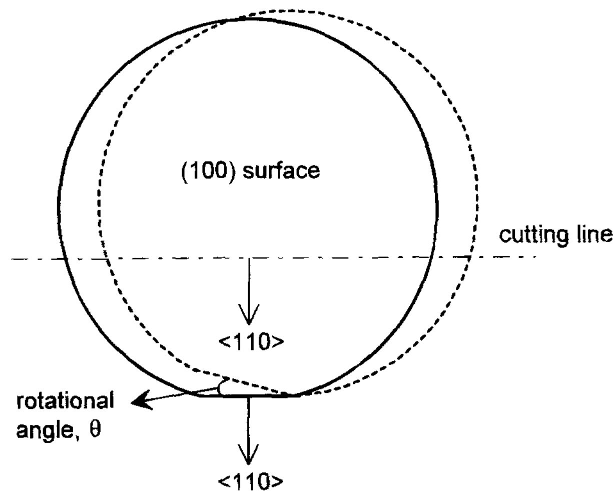

Fig. 3. Illustration of a (100) wafer bonding and cutting angle.

Experimental

Figure 1 shows the procedure of sample preparation schematically. We used commercially available n-type (100) CZ (Czochralski grown) Si wafers which are 4 in. in diam, 525 μm in thickness, and 5.3 ~ 7.1 Ω cm in resistivity. The CZ wafer contains 7.5×10^{17} cm^{-3} interstitial oxygen atoms, which is measured with Fourier transform infrared (FTIR) spectroscopy according to ASTM F121-83. [17]

Prior to bonding, we cleaned the wafers using the modified RCA method, omitting the preliminary cleaning step.[18] Subsequently, we dipped the wafers into the hydrophilizing solution (H_2O:H_2O_2:NH_4OH = 6:1:4 in volume ratio) for 2 min at 57°C to form hydrophilic layers on the wafer surface. Then, we rinsed the wafers in deionized water and dried using a spin-dryer. Figure 2a and b shows the atomic force microscopic (AFM) images of the surface roughness of Si wafers before and after the modified RCA cleaning and the hydrophilizing treatment. The average roughness was calculated to be increased from 0.603 to 0.838 nm after the chemical treatment. We think this increase in roughness was originated from slight etching and oxidation of Si by $NH_4OH/H_2O_2/H_2O$-based cleaning and hydrophilizing solutions.[19-21]

Next, two wafers were contacted to each other as shown in Fig. 3 at room temperature in N_2 atmosphere having a rotational angle of θ = 0 or 5°. Then, we annealed the weakly bonded wafer pairs at 700 ~ 1200°C in N_2 for 30 min ~ 10 h. Most of our analyses were done with the data obtained at 1100°C because almost all studies on oxide stabilization-disintegration-spheroidization have been done around this temperature.[4-9,22] Data obtained at other temperatures were also analyzed to support the results drawn from the data obtained at 1100°C annealing temperature.

The bonded wafer pairs were cut parallel to the (110) primary flat of one wafer with a diamond saw like Fig. 3, and were etched anisotropically in 44 g KOH-100 ml H_2O solution for 4 min at 90°C. [3] Also, we prepared the bonded wafer pairs for TEM observation. The list of all the samples used in this experiment is shown in Table I.

Results and Discussion

Figure 4a and b shows the bonding interfaces etched in KOH solution for the samples named S1 and S2 in Table I, respectively. We can clearly observe (111) facets in both cases. The crystallographic features of the facets were calculated previously based on the geometry of the facets.[3] Figure 5 is a surface profile (scanned by SAS Tech Co., Nanosurf 488) for the KOH-etched (110) cross section of the sample S1. The ratio of height of the facet to its width is 0.35, which indicates the facet is made of (111) crystal planes. At the bonding interface of sample S2, which is annealed for a longer time than sample S1, the roof-shaped peaks (which look like a thin line in the sample S1) began to disappear randomly. This created a broken line of the roof-shaped peaks at the bonding interface.

For investigation of the difference between the two samples near the bonding interface, we employed TEM analysis. Figure 6a is the TEM photograph of the bonding interface for sample S1. It seems apparent that the interfacial oxide of the sample has undergone a disintegration process. The thickness of the oxide islands is approximately 7 to 9 nm and their lengths range from 15 to 45 nm.

Now, we discuss briefly the interfacial oxide existing at the bonding interface. RCA cleaning produces a native ox-

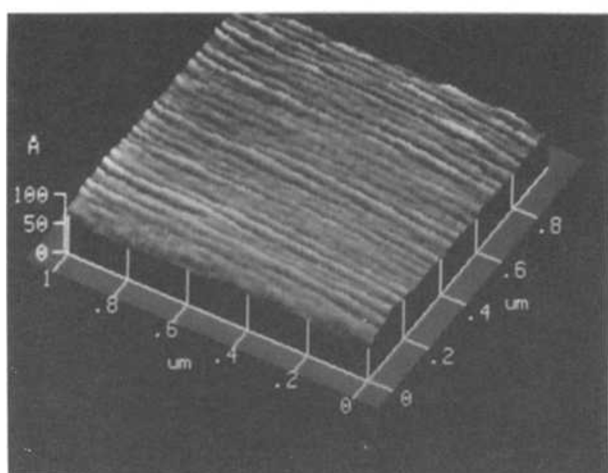

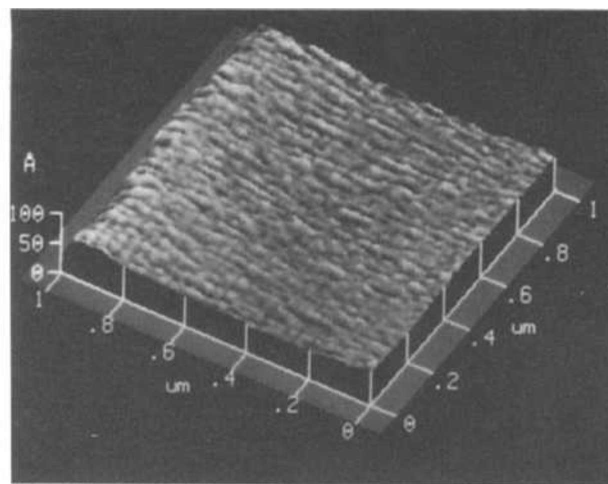

Fig. 2. Surface roughness of Si wafers used in this experiment (a, left) before and (b, right) after the modified RCA cleaning/hydrophilizing step.

Downloaded on 2014-03-19 to IP 163.152.61.222 address. Redistribution subject to ECS terms of use (see ecsdl.org/site/terms_use) unless CC License in place (see abstract).

Table I. Sample specifications.

Sample number	Oxygen concentration (cm^{-3})	Surface roughness (after chemical treatment) [nm (rms)]	Rotational angle (deg)	Annealing condition
S1	7.5×10^{17}	0.838	<0.3	1100°C, 30 min
S2	7.5×10^{17}	0.838	<0.3	1100°C, 3 h
S3	7.5×10^{17}	0.838	5.0 ± 0.2	1100°C, 3 h
Others	7.5×10^{17}	0.838	<0.3 or 5.0 ± 0.2	700 ~ 1200°C, 30 min ~ 10 h

ide film with thickness of 1.3 ~ 1.5 nm on the surface of Si wafer.[21,23] Therefore, a thin interfacial oxide layer exists between two bonded wafers cleaned with the RCA method. The hydrophilizing solution has a tendency to oxidize the wafer surface slightly and there is a thin interface phase with OH groups between the oxide layers. Because of the above reasons, the total thickness of the amorphous oxide layer between two bonded wafers is usually 3.5 ~ 4 nm at room temperature.[4-9,24]

The local diffusion model used by Ahn *et al.*[4,5] suggests that the interfacial oxide layer is disintegrated and finally spheroidized into a two-dimensional hexagonal lattice of spheroids during a long-time annealing at high temperature. This phenomenon occurs in both CZ and FZ (float zone) wafers independent of the oxygen concentration. But Abe *et al.*[7] and Ishigami *et al.*[10] claimed that the interstitial oxygens in bulk Si diffused out toward the bonding interface and contributed to the growth of the oxide layers in CZ wafers, which have a much higher concentration of interstitial oxygens than FZ wafers, in the temperature range of 1000 to 1200°C. However, Ling and Shimura[8] observed that the thickness of the layers decreased with the increasing bonding temperature in the temperature range of 200 to 600°C, and remained constant in the range of 600 to 1200°C in both CZ and FZ Si wafer pairs. In their recent report,[9] they observed that the oxide layer in a CZ wafer pair was structurally more stable than that in an FZ wafer pair. They also observed that the effect of oxygen outdiffusion toward the bonding interface on the oxide layer formation was negligible, which was contradictory to the Abe *et al.* results.[7]

In our experiment, the interfacial oxide was disintegrated as shown in Fig. 6a even though the wafer was annealed for only 30 min at 1100°C. After being annealed for 3 h at the same temperature, the oxide layer appeared to be spheroidized near the bonding interface of sample S2 as shown in Fig. 6b. This observation was in agreement with the model of Ahn *et al.* which predicted the spheriodization of the layers after a high temperature and long-time annealing. The diameters of the largest oxide spheroid were measured to be ~12 nm as shown in Fig. 6c. Based on the above results, we concluded that the generation mechanism of (111) facets at the KOH-etched bonding interface cannot be explained simply by the assumption of Mitani *et al.* which claims that native oxides act as an etch mask.[3]

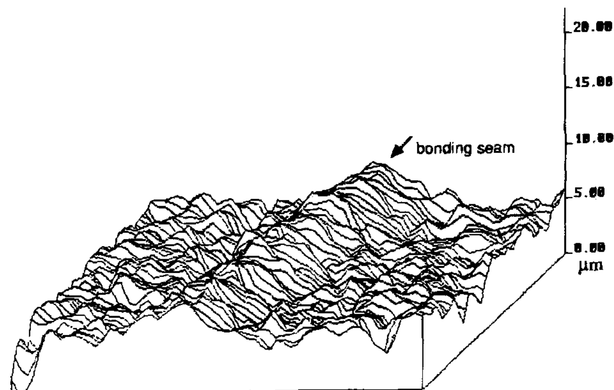

Fig. 5. Surface profile of the KOH-etched (110) cross section of sample S1; (measured area: 60 × 50 μm).

Next, we investigated the shape of the (111) facet structure when the native interfacial oxide layer is stabilized at the bonding interface. According to Ahn *et al.*[4,5] screw dislocations were generated near the bonding interface when two wafers were bonded with a rotational angle θ around their common axis perpendicular to the wafer planes as shown in Fig. 3. These dislocations prevented energetically the interfacial oxide from disintegration and spheroidization. Typically, the critical angle θ_{crit} above which the interfacial oxide was stabilized had a value of 1° ~ 5° depending on the Si/SiO_2 interface energy, shear modulus, and Burgers vector of the screw dislocation.

Figure 7 shows cross-sectional TEM photographs for sample S3 which was bonded with a rotational angle of 5° and annealed at 1100°C for 3 h in N_2 atmosphere. The oxide layer is generally stable over the whole area, even though it is partially broken in small areas, as shown in Fig. 7a. The thickness of the interfacial oxide is measured to be ~4.2 nm with a fluctuation of 0.4 nm as shown in Fig. 7b. This value is close to the one obtained by Widdershoven *et al.*[6] They observed a 4.4 nm thick amorphous layer between a bonded FZ and CZ wafer pair annealed for 3 h at the temperature of 1100 ~ 1125°C in N_2 atmosphere. Therefore, it seems likely that the rotational misorientation method can stabilize the interfacial oxide.

Next, we etched the (110) cross section of sample S3 using the KOH-H_2O solution. Figure 8a shows the etched bonding interface. One side of the etched surface has a (110) plane and the other side has a 5°-rotated (110) plane. We can observe a very thick line of (111) facet structure at the bonding interface and depict the crystallographic feature in Fig. 8b. It seems clear that the interfacial oxide acts

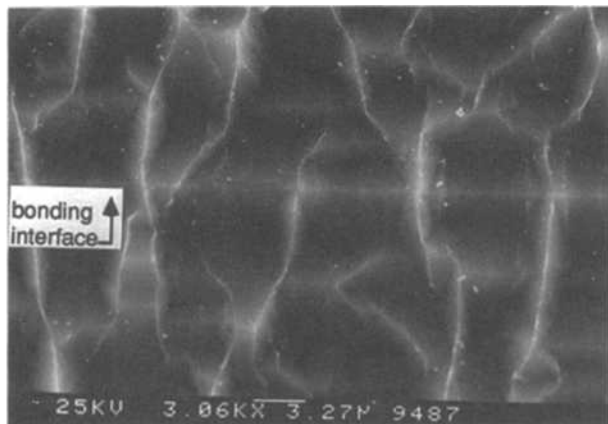

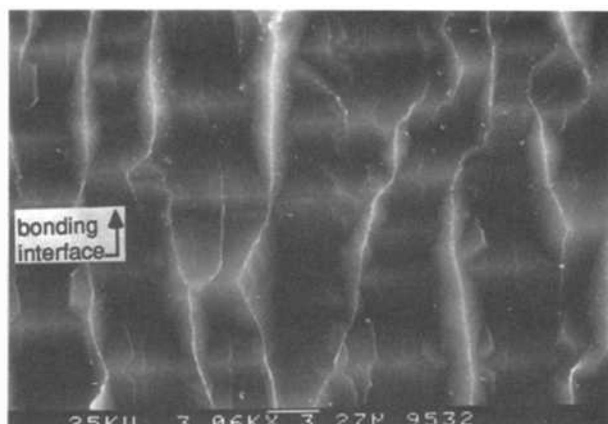

Fig. 4. SEM photographs of the KOH-etched (110) bonding interface for samples (a, left) S1 and (b, right) S2.

Downloaded on 2014-03-19 to IP 163.152.61.222 address. Redistribution subject to ECS terms of use (see ecsdl.org/site/terms_use) unless CC License in place (see abstract).

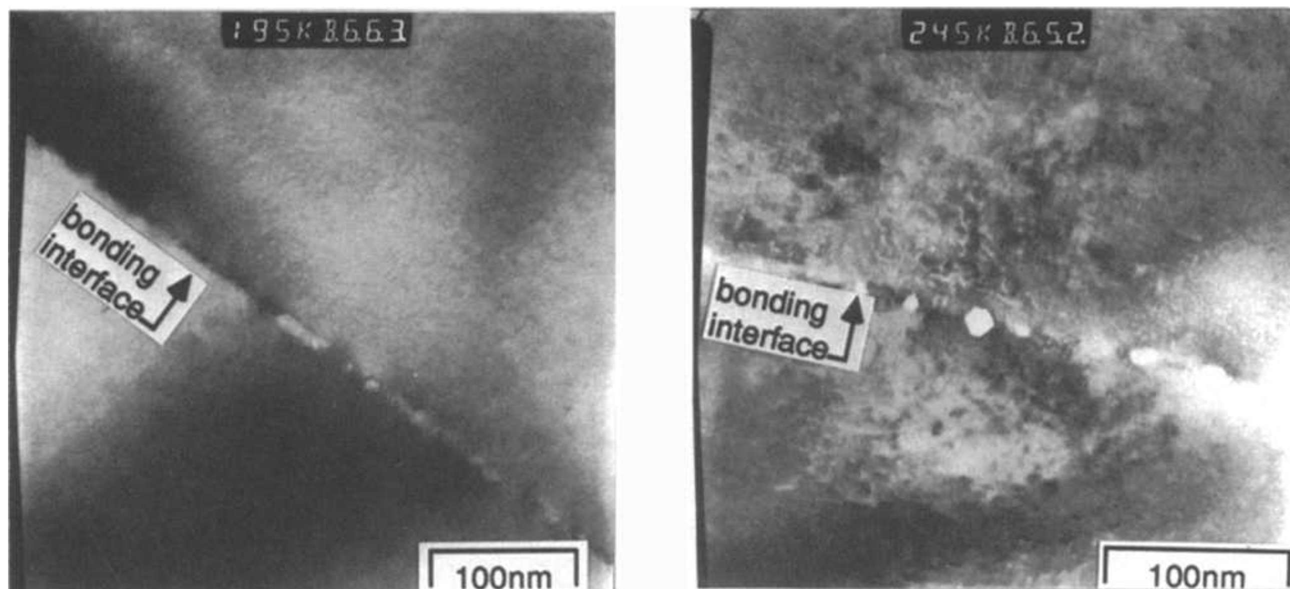

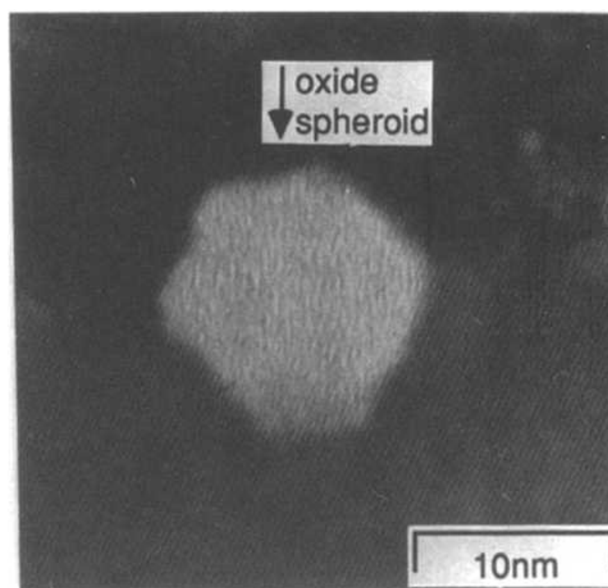

Fig. 6. TEM photographs of the bonding interface of sample (a, above) S1, (b, top right) S2, and the magnified view of the oxide spheroid in sample (c, right) S2.

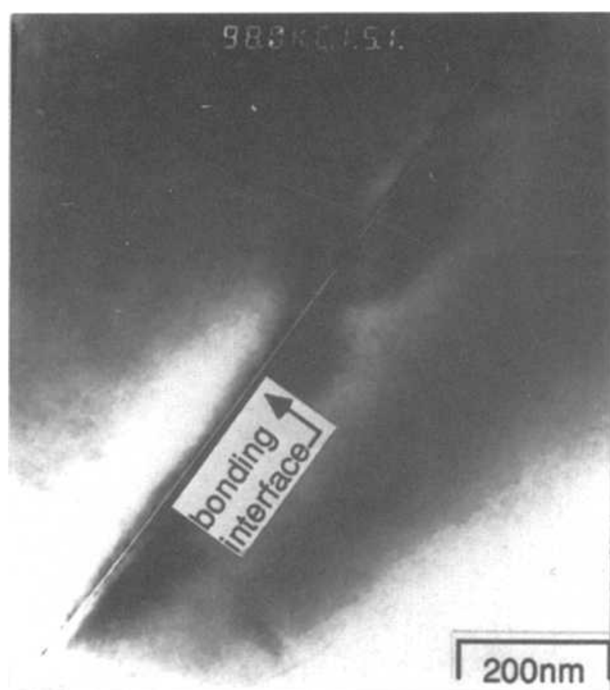

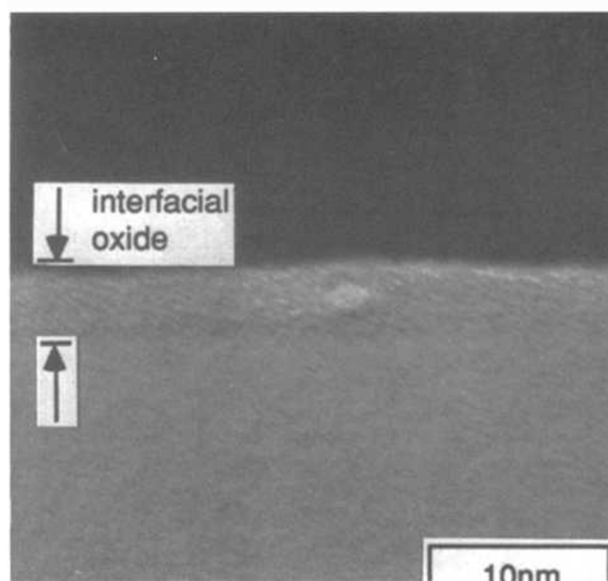

Fig. 7. (a, left) TEM and (b, right) HRTEM photographs of the bonding interface for sample S3.

Downloaded on 2014-03-19 to IP 163.152.61.222 address. Redistribution subject to ECS terms of use (see ecsdl.org/site/terms_use) unless CC License in place (see abstract).

as an etch mask during KOH etching and this is in agreement with the assumption of Mitani *et al.*[3]

Even for well-aligned wafer pairs such as samples S1 and S2, the (111) facet structure shown in Fig. 8a also appears in a prevoid region. The prevoid region is defined as a region where previously existing voids disappear after an annealing and a well-contacted region is defined as a region without voids before and after the annealing process.[25] Figure 9a shows the KOH-etched boundary between the prevoid region and the well-contacted region under Nomarski mode for sample S2. The thick (111) facet structure has clearly remained on the prevoid region as shown in Fig. 9b which is a magnified picture of the left side of Fig. 9a. This phenomenon can be explained assuming that the disintegration and the spheroidization processes are relatively slower in the prevoid region than in the well-contacted region. After suffering from further annealing at 1100°C for 7 h (total 10 h), the shape of the facet structure of the prevoid region became similar to the one shown in Fig. 4b.

To determine the cause of the (111) facet formation, we carried out the KOH anisotropic etching on the surface of commercially available p-type (110) CZ Si wafers. The wafers are 2 in. in diam, 280 μm in thickness, and 26.0 ~ 30.0 Ω cm in resistivity and have a (110) reference flat. They are etched for 4 min in the same KOH solution as previously used. Figure 10a shows the KOH-etched shape of a typical mirror-polished surface of the (110) Si wafer. Many facets are observed on the etched (110) surface, and they are 35.26° off from the (110) reference flat which means the facets consist of (111) crystal planes.[26] The (111) facets have similar shapes with the ones observed at the KOH-etched (110) cross section of sample S2 shown in Fig. 4b. However, their sizes are much larger than those in Fig. 4b. Figure 10b is a photograph of a KOH-etched surface of the mechanically damaged (110) surface. This surface was scratched perpendicular to the direction of the trace of (111) planes using an abrasive paper (No. 150 Cw). Figure 10b indicates that the length of facet is dependent on the roughness of the surface. The length of the (111) facet on the damaged (110) surface is determined by the unstable etching rate which is locally varied with the nonuniform surface roughness. Therefore, we can conclude that the (111) facets on the (110) surface are generated as a result of a disturbance in the etching rate related to the surface roughness or nonuniformity.

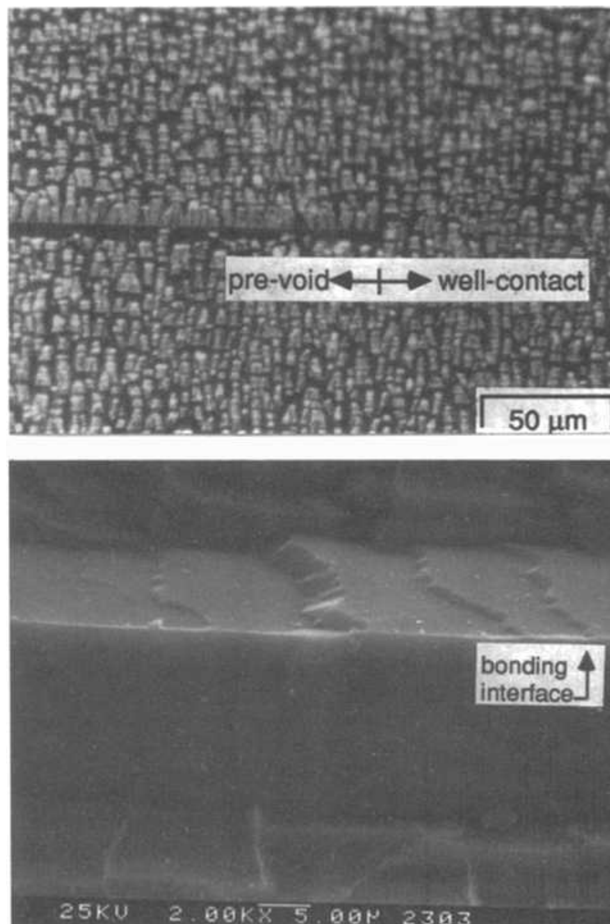

Fig. 9. Photograph of the boundary of the prevoid region and the no-void region under (a, top) Nomarski mode and (b, bottom) the magnified SEM photograph of the prevoid region for the KOH-etched sample S3.

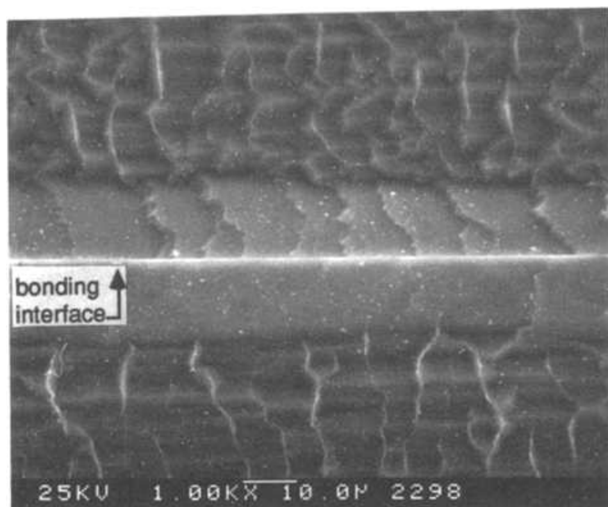

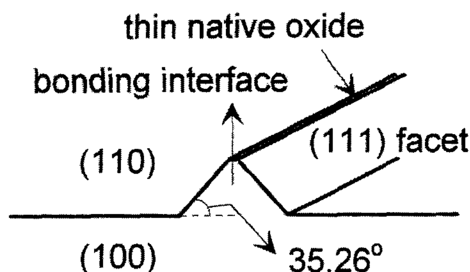

Fig. 8. (a, top) SEM photograph and (b, bottom) crystallographic illustration of the KOH-etched (110) bonding interface for sample S3.

Finally, we measured the surface energy γ from the wafer edge by the crack propagation method designed by Maszara *et al.*[15] using a razor blade with thickness of $2y$ = 430 μm. We evaluated the surface energy using

$$\gamma = \frac{3}{8} E \frac{t^3 y^2}{L^4}$$

with E being the modulus of elasticity, t the thickness of the wafer, and L the crack length. The L value was determined by using ultrasonic microscope (Testech LS-240 scanning and recording system)[25] after inserting the razor blade between the two bonded wafers. Because this method has a 10% margin of error, we tested five pieces per sample and recorded the range from the minimum to the maximum values for each sample.

All the results obtained from this experiment are summarized in Table II. We deduced three kinds of interesting results from the data in Table II. First, each distinct shape of the roof-shaped peak of facet structures at bonding interface can be mapped to one of three conditions of the interfacial oxide as follows. Thick line can be mapped to stabilization, thin line to disintegration, and broken line to spheroidization. If the annealing temperature is not high enough to disintegrate the interfacial oxide (in our study, this critical temperature is observed to be ~900°C in agreement with the report by Wolstenholme *et al.*[22]) or the oxide is stabilized through the rotational misorientation method, the shapes of KOH-etched (111) facet at interface always appear to be thick lines.

Downloaded on 2014-03-19 to IP 163.152.61.222 address. Redistribution subject to ECS terms of use (see ecsdl.org/site/terms_use) unless CC License in place (see abstract).

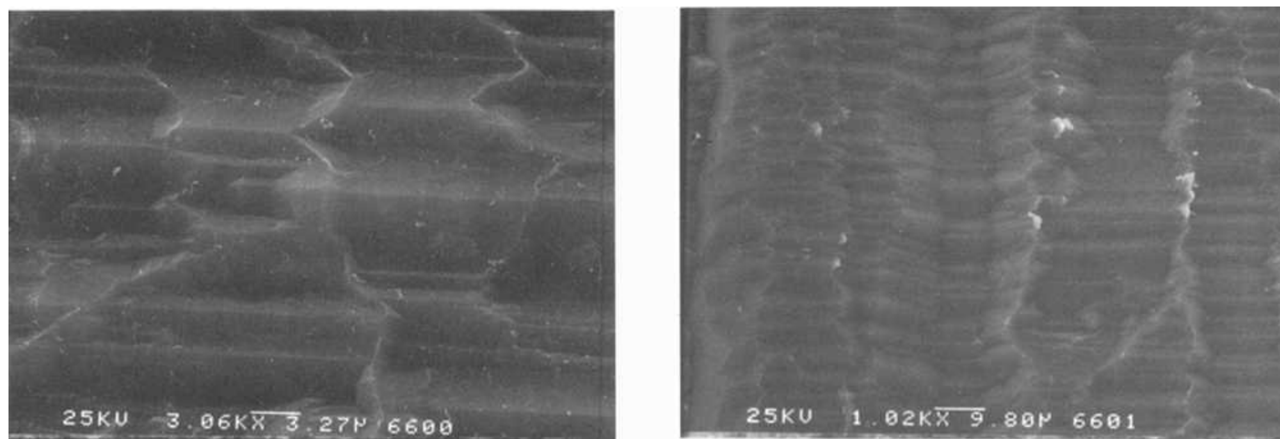

Fig. 10. SEM photographs of the KOH-etched surface of a typical (a, left) mirror-polished and (b, right) mechanically damaged (110) Si wafers.

Second, most of the interfacial oxide existing at the bonding interface of well-aligned wafer pairs were disintegrated and spheroidized through a high temperature annealing process >900°C.

Third, we found that the surface energy (bonding strength) is somewhat dependent on the condition of interfacial oxide. That is, the surface energy was increased as the interfacial oxide layer became gradually disintegrated and spheroidized. Even the 180 min-annealed sample S3 with stabilized oxide had lower surface energy than the 30 min-annealed sample S1 with disintegrated oxide.

For sample S3, the bonding interface of the silicon wafers are composed of Si-O-Si bonds, but the Si-O-Si bonds are gradually replaced by Si-Si bonds for samples S1 and S2 during the disintegration process of the interfacial oxide. Therefore, we can guess that Si-Si bonds are stronger than the Si-O-Si bonds and the bonding strength is increased as the area of oxide layer decreases. Also some authors have shown that, when compared with the bonded Si-Si structure, the bonded Si-SiO_2-Si structure has a weaker bonding strength caused by some reasons, such as a relatively higher roughness of SiO_2 film[1] and repulsive force among oxygen atoms.[27] However, further study is required to demonstrate a clear relationship between the surface energy and the condition of interfacial oxide.

Conclusion

We investigated the condition of interfacial oxide in directly bonded (100) CZ Si wafer pairs by observing the shape of (111) facets generated at the (110) cross section after KOH etching. We found that the various shapes of (111) facets at bonding interface (thick line, thin line, broken line) show the respective oxide condition (stabilization, disintegration, spheroidization).

Also we confirmed, based on the results obtained by the observation of the KOH-etched bonding interface and TEM evaluation, that most of the interfacial oxide existing at the bonding interface of well-aligned wafer pairs were disintegrated and spheroidized through a high temperature (900°C) annealing process.

The new KOH etch-based testing method can provide a more comprehensible picture of the interfacial oxide condition and is easy to implement when compared with a conventional HRTEM observation. We believe that this method will be useful in testing various devices fabricated by the wafer bonding technique. Some of the examples are power devices fabricated by bonding two Si wafers with two different conduction types (N/P or N^+/P^+), the devices in which the current flows across the bonding interface, and silicon-on-insulator structure with a thin buried oxide layer.

Table II. Summarization of the results.

Annealing temp.-time (°C)-(min)	Rotational angle (degree)	Shapes of (111) facet	Interfacial oxide (by TEM)	Surface energy (erg cm^{-2})	Remarks
700-180	<0.3	Thick[a]	—[e]	—	
700-600	<0.3	Thick	Stabilization	160 ~ 280	
800-180	<0.3	Thick	—	—	
800-600	<0.3	Thick	Stabilization	180 ~ 280	
900-180	<0.3	Thin[b]	—	—	
900-600	<0.3	Thin-broken[d]	Disintegration	250 ~ 320	
1000-30	<0.3	Thin	—	—	
1000-180	<0.3	Thin-broken	—	—	
1000-180	~5.0	Thick	—	—	
1000-600	<0.3	Broken[c]	Spheroidization	490 ~ 610	
1000-600	~5.0	Thick	Stabilization	280 ~ 380	
1100-30	<0.3	Thin	Disintegration	400 ~ 600	S1
1100-180	<0.3	Broken	Spheroidization	550 ~ 900	S2
1100-180	<0.3	Thick	—	150 ~ 300	Prevoid
1100-180	~5.0	Thick	Stabilization	300 ~ 450	S3
1100-600	<0.3	Broken	—	—	
1100-600	<0.3	Broken	—	520 ~ 720	Prevoid
1100-600	~5.0	Thick	Stabilization	—	
1200-30	<0.3	Broken	—	—	
1200-180	<0.3	Broken	—	—	
1200-180	~5.0	Thick	—	—	
1200-600	<0.3	Broken	—	—	
1200-600	~5.0	Thick			

[a,b,c] The "thick," "thin," and "broken" lines mean the shapes of peak of (111) facets at the bonding interface like the photographs in Fig. 8a, Fig. 4a, and Fig. 4b, respectively.
[d] The "thin-broken" means a coexisted shape of the "thin" and "broken" line-shaped (111) facet peak.
[e] The TEM observation or measurement of surface energy was not carried out.

Downloaded on 2014-03-19 to IP 163.152.61.222 address. Redistribution subject to ECS terms of use (see ecsdl.org/site/terms_use) unless CC License in place (see abstract).

Finally, we found that the bonding strength of the bonded wafer pairs was increased as the interfacial oxide was disintegrated and spheroidized. We hypothesized that this phenomenon was due to the difference in binding energy between Si-O-Si and Si-Si bond, but more detailed study is needed to specify it.

Manuscript submitted Sept. 8, 1994; revised manuscript received Sept. 12, 1994.

Korea Institute of Science and Technology assisted in meeting the publication costs of this article.

REFERENCES

1. W. P. Maszara, *This Journal*, **138**, 341 (1991).
2. S. J. Yun, K.-Y. Ahn, K.-S. Yi, and S.-W. Kang, *ibid.*, **139**, 2326 (1992).
3. K. Mitani, D. Feijoo, G. Cha, and U. M. Gösele, *Jpn. J. Appl. Phys.*, **31**, 969 (1992).
4. K.-Y. Ahn, R. Stengl, T. Y. Tan, and U. Gösele, *J. Appl. Phys.*, **65**, 561 (1989).
5. K.-Y. Ahn, R. Stengl, T. Y. Tan, U. Gösele, and P. Smith, *Appl. Phys. A*, **50**, 85 (1990).
6. F. P. Widdershoven, J. Haisma, and J. P. M. Naus, *J. Appl. Phys.*, **68**, 6253 (1990).
7. T. Abe, A. Uchiyama, K. Yoshizawa, Y. Nakazato, M. Miyawaki, and T. Ohmi, *Jpn. J. Appl. Phys.*, **29**, L2315 (1990).
8. L. Ling and F. Shimura, *J. Appl. Phys.*, **71**, 1237 (1992).
9. L. Ling and F. Shimura, *This Journal*, **140**, 252 (1993).
10. S. I. Ishigami, Y. Kawai, H. Furuya, T. Shingyouji, and Y. Saitoh, *Jpn. J. Appl. Phys.*, **32**, 5463 (1993).
11. H. Himi, M. Matsui, S. Fujino, and T. Hattori, *ibid.*, **33**, 6 (1994).
12. R. D. Black, S. D. Arthur, R. S. Gilmore, N. Lewis, E. L. Hall, and R. D. Lilquist, *J. Appl. Phys.*, **63**, 2773 (1988).
13. O. Okabayashi, H. Shirotori, H. Sakurazawa, E. Kanda, T. Yokoyama, and M. Kawashima, *J. Crystal Growth*, **103**, 456 (1990).
14. M. Shimbo, K. Furukawa, K. Fukuta, and K. Tanzawa, *J. Appl. Phys.*, **60**, 2987 (1986).
15. W. P. Maszara, G. Goetz, A. Caviglia, and J. B. McKitterick, *ibid.*, **64**, 4943 (1988).
16. F. Sugimoto and Y. Arimoto, *Jpn. J. Appl. Phys.*, **31**, 975 (1992).
17. ASTM standards, Vol. 10.05, Section 10, American Society for Testing and Materials, Philadelphia (1989).
18. W. Kern, *Semiconductor International*, 94 (April 1984).
19. J. E. A. M. van der Meerakker and M. H. M. van der Straaten, *This Journal*, **137**, 1239 (1990).
20. H. Kobayashi, J. Ryuta, T. Shingyouji, and Y. Shimanuki, *Jpn. J. Appl. Phys.*, **32**, L45 (1993).
21. R. C. Henderson, *This Journal*, **119**, 772 (1972).
22. G. R. Wolstenholme, N. Jorgensen, P. Ashburn, and G. R. Booker, *J. Appl. Phys.*, **61**, 225 (1987).
23. B. Soerowirdjo and P. Ashburn, *Solid-State Electronics*, **26**, 495 (1983).
24. R. Stengl, T. Tan, and U. Gösele, *Jpn. J. Appl. Phys.*, **28**, 1735 (1989).
25. B. K. Ju, M. H. Oh, and K. H. Tchah, *J. Mater. Sci.*, **28**, 1168 (1993).
26. D. F. Weirauch, *J. Appl. Phys.*, **46**, 1478 (1975).
27. T. Abe, T. Takei, A. Uchiyama, K. Yoshizawa, and Y. Nakazato, *Jpn. J. Appl. Phys.*, **29**, L2311 (1990).

The Effect of the Thermal History of Czochralski Silicon Crystals on the Defect Generation and Refresh Time Degradation in High Density Memory Devices

Sun S. Kim

Texas Instruments, Incorporated, Dallas, Texas 75265

W. Wijaranakula*

Shin-Etsu, SEH America, Incorporated, Vancouver, Washington 98682

ABSTRACT

The effect of the thermal history of Czochralski silicon crystals on the generation of crystallographic defects and refresh time degradation in high density memory devices was investigated. The result from an electron microscopic analysis shows that the oxide precipitates with a ring-type pattern around the crystal periphery, typically observed in the bottom section, have a polyhedral-shaped morphology. The grown-in oxide polyhedra are thermodynamically stable during the high temperature device processing steps and hence could be nucleated at temperatures above 1150°C. The present result also indicates that the refresh time degradation in trench-type memory devices is directly related to the grown-in oxide polyhedra located in the device active region. Based upon the present analysis, the formation of the oxide precipitate ring in the bottom section of the crystal is hypothesized to be caused by radiative heating during and after the crystal tailing-off process.

Introduction

The leakage of stored charge is one of the major causes of failure in dynamic random access memory (DRAM) devices. The capacitors lose their charge due to various leakage current sources. Cells with low retention times fail due to leakage currents generated from centers which are located in the space charge region of the storage capacitor. In Czochralski (CZ) silicon wafers, oxide microprecipitates and D-defects introduce energy levels in the bandgap and are considered to be the possible sources of the leakage currents.[1-3] Since the generation of oxide microprecipitates and D-defects depends upon the thermal history of the crystal and its growth conditions, an improvement in the reliability and performance of the memory devices can be achieved by establishing a good understanding of the device degradation mechanisms which are attributed to the crystallographic grown-in defects.

It is well accepted that the generation of the crystallographic grown-in defects is strongly affected by the thermal history of the crystals. The effect of an *in situ* annealing in the growth furnace after the crystal tailing-off process has been investigated and found to have a pronounced effect on the generation of crystallographic defects such as oxidation induced stacking faults (OSFs) and other microdefects during the subsequent high temperature annealing.[4-5] In p-type silicon, the OSF formation with a ring-type pattern, particularly in the bottom section of the crystal, is observed to be susceptible to the crystal cooling down conditions after the tailing-off process.[4] Hasebe *et al.*[6] elucidated the OSF formation in the annular zone to be associated with oxide precipitates which were nucleated at 1150°C or higher. A two oxygen species model consisting of

* Electrochemical Society Active Member.

Downloaded on 2014-03-19 to IP 163.152.61.222 address. Redistribution subject to ECS terms of use (see ecsdl.org/site/terms_use) unless CC License in place (see abstract).